THE AMERICAN SOCIETY OF MECHANICAL ENGINEERS
345 E. 47 St., New York, N.Y. 10017

A Model For Thermally Driven Heat and Air Transport in Passive Solar Buildings

G. F. JONES, Los Alamos National Laboratory
J. D. BALCOMB, Los Alamos National Laboratory
D. R. OTIS, University of Wisconsin-Madison

ABSTRACT

A model for transient interzone heat and air flow transport in passive solar buildings is presented incorporating wall boundary layers in stratified zones, and with interzone transport via apertures (doors and windows). The model includes features that have been observed in measurements taken in more than a dozen passive solar buildings. The model includes integral formulations of the laminar and turbulent boundary layer equations for the vertical walls which are then coupled to a one-dimensional core model for each zone. The cores in each zone exchange mass and energy through apertures that are modeled by an orifice type equation. The procedure is transient in that time dependence is retained only in the core equations which are solved by an explicit method. The model predicts room stratification of about 2°C/m (1.1°F/ft) for a room-to-room temperature difference of 0.56°C(1°F) which is in general agreement with the data.

NOMENCLATURE

a	$2/(n+1)$, dimensionless
A_D	H/D, dimensionless
A_L	H/L, dimensionless
A_W	H/W, dimensionless
B	variable defined by Eq. (9) and (15), dimensionless
C_1-C_8	coefficients defined by Eq. (17), dimensionless
c_p	specific heat, J/kg K
C_r	reference-pressure relaxation coefficient, dimensionless
D	core breadth, m
E_1-E_5	coefficients defined by Eq. (30), dimensionless
f	variable defined by Eq. (5), K/m
g	acceleration of gravity, m/s^2
G	vertical volumetric flowrate in core, m^3/s
$\hat{G}$	$G/\kappa H$, dimensionless
H	height of rooms, m
I	integrals used in boundary-layer equations, dimensionless
k	thermal conductivity of air, W/mK
L	core length, m
n	reciprocal exponent in turbulent boundary-layer profiles, dimensionless
N	defined by Eq. (10), dimensionless
NN	maximum number of nodes in core, dimensionless
Nu_L	heat loss coefficient, dimensionless
p	pressure, N/m^2
$\hat{p}$	$p/(\rho_0 gH/2)$, dimensionless
Pr	Prandtl number, ν/κ, dimensionless
q,r	exponents defined by Eq. (16)
q_w	wall heat flux, W/m^2
Q	horizontal volumetric flowrate in core, m^3/s
$\hat{Q}$	$Q/\kappa H$, dimensionless
R	integral continuity residual, See Eq. (27), dimensionless
Ra	Rayleigh number, $g\beta H^4 \alpha_e S/\nu\kappa k$, dimensionless
S	heat flux at vertical wall, W/m^2
t	time, s
T	temperature, K
u	vertical velocity in boundary layer, m/s
U_L	loss coefficient from inside surface of vertical wall to outside, W/m^2K
W	aperture breadth, m
x	vertical coordinate in rooms, m
y	Horizontal coordinate in rooms, m

Greek Symbols

α_e	effective absorptance of wall if S is from a radiant source, dimensionless
β	coefficient of thermal expansion, 1/K
δ	boundary-layer thickness, m
η	y/δ, dimensionless
θ	$(T_\infty - T_a)/(\alpha_e S H/k)$, dimensionless
κ	thermal diffusivity, m^2/s
λ	$\delta Ra^{1/5}/H$, dimensionless
ν	kinematic viscosity, m^2/s
ξ	x/H, dimensionless
ρ	density, kg/m^3
τ	$\kappa t/H^2$, dimensionless
τ_w	wall shear stress, N/m^2

Presented at the Winter Annual Meeting
Miami Beach, Florida—November 17-21, 1985

ψ $T_\infty/(g_e S H/k)$, dimensionless
ω boundary-layer characteristic velocity, m/s
Ω $\omega/(\kappa Ra^{2/5}/H)$, dimensionless

Subscripts

a ambient
b bottom of aperture
ℓ laminar
L based on horizontal spacing, L
0 reference value
s source room
t turbulent
u top of aperture
ΔT based on ΔT
∞ core

Superscripts

' from core to boundary layer
" from core to aperture

INTRODUCTION

Natural convection plays a major role in the transport of heat in most passive solar buildings, especially those that employ sunspaces or atria for solar heat collection. The convective exchange typically involves doors, halls, stairways, and interior windows (referred to as **apertures** in this paper). To gain greater understanding of this complex problem, the Los Alamos National Laboratory (LANL) has measured temperature, velocity, and solar radiation and done flow visualization in more than a dozen full-scale buildings of various designs (1-3). Data show that modest temperature differences between rooms result in large air circulations which carry substantial energy. For example, in moderate sized residential buildings with room temperature differences ranging from 1.76 to 5.6°C (3 to 10°F), air circulation rates of 0.22 to 1.06 m^3/s (470 to 2240 cfm) and energy flow rates of 0.63 to 6.2 kw (2140 to 21,000 Btu/h) have been observed.

Building geometry and aperture flow areas have a major influence on thermal performance and comfort, and a simulation model would be a useful tool. This requires development of models for each convection process (element models), and a combination of the elements into a building simulation. Some element models are already well established. For example, aperture flows have been shown to agree quite well with predictions of a simple orifice model (sometimes referred to as a "Bernoulli model") (2,4,5) and a number of boundary-layer analyses have also been reported for natural convection on vertical and horizontal walls. In addition, there have been a considerable number of studies, both experimental and theoretical to model the heat exchange in rectangular enclosures and some in two-room enclosures. But, full-scale buildings are much more complex, and existing analyses are too restricted to be of much quantitative use.

The proposed model is an attempt to meet this need by assembling elements in series and parallel so that what is in reality a three-dimensional phenomenon can be reduced to an assembly of one-dimensional elements. This paper treats a minimum number of elements for simplicity, but encompasses many of the important effects observed during the building monitoring program. It is anticipated that other features will be incorporated as data become available.

BACKGROUND

The proposed model concerns natural convection in large thermally stratified enclosures (buildings) having interior partitions and subject to a variety of possible thermal boundary conditions at the walls. The following review briefly focuses on stratification, the type of thermal boundary condition imposed, transition to turbulence, and flow blocking from partitions, and their effects on heat transfer in buildings.

Since Batchelor's (6) pioneering study of two-dimensional natural convection in a rectangular enclosure in 1954, there have been numerous experimental and analytical investigations of this topic. Elder's (7) experiments for laminar natural convection at high Prandtl and Rayleigh numbers and with constant temperature vertical walls (CWT) show a nearly constant core temperature gradient which increases with Rayleigh number and reaches a maximum value at $Ra_{\Delta T,L} = 10^5$. A marked increase in the core temperature gradient is noted in the fluid next to the top and bottom walls of the enclosure due to horizontal boundary layers that flow along these surfaces. Many other investigations have been reported (8-15) for these same geometry and boundary conditions, however, the constant wall temperature boundary condition (CWT) is not the one experienced in most buildings; rather, it more often tends to approach constant wall heat flux (CWHF) for solar irradiated glazings, or a combination of constant heat flux and heat loss through walls or windows to the ambient.

Gill (16) obtained an analytical solution with a CWHF boundary condition for laminar natural convection on a vertical flat plate in the limit $Pr \to \infty$, and he showed that the boundary layer thickness became constant. Kimura & Bejan (17) applied the Oseen type linearization (also used by Gill but for the CWT boundary condition) to the rectangular enclosure with a CWHF boundary condition. They concluded that the vertical wall boundary layers had constant thickness, and the core was motionless and linearly stratified. The stratification temperature gradient was found to be proportional to $Ra^{-1/9}$ (based on enclosure height). Similar results were obtained by Evans, Reid and Drake (18) for transient natural convection with CWHF boundaries in a vertical circular enclosure.

A numerical study of high Rayleigh number laminar and turbulent natural convection having CWT boundaries was carried out by Markatos and Pericleous (19) for $Ra_{\Delta T,L}$ up to 10^{16}, and by Bauman, et al. (20) and Gadgil, et al. (21) for $Ra_{\Delta T,L}$ up to $\sim 10^{10}$. The latter study reports transitional flow to persist for $Ra_{\Delta T,L}$ up to 1.3×10^{10}. Using the governing equations for laminar flow, they predicted local temperatures and heat fluxes, and mean Nusselt numbers that were in good agreement with experimental data.

Several investigations of natural convection in enclosures driven by mixed boundaries (one vertical wall CWT, the other CWHF) have been reported. Emery and Chu (22) developed an approximate analytical solution for heat transfer in a large aspect ratio enclosure having mixed boundary conditions. They considered the energy transport between the independent vertical boundary layers on the heated and cooled walls to be coupled by an isothermal core having a temperature midway between the mean wall temperatures. Their analysis agreed well with data for $Ra_{\Delta T,L} > 3 \times 10^5$ and for aspect ratios (height/length) of 10 and greater.

MacGregor and Emery (23) also tested enclosures with mixed boundaries, and they found a 30% increase in heat transfer versus the CWT condition. They also show aspect ratio has only a slight effect on heat transfer for $Ra_{\Delta T,L} > 10^9$. They observed transition at Rayleigh numbers of $O(10^{10})$.

Some experiments have been reported for partially divided enclosures and for full-scale buildings (1-5,24-31). Nansteel and Greif (27) used a water-filled enclosure divided by a vertical partition extending part-way down from the ceiling. The vertical end-walls were maintained at two different temperatures, and the Rayleigh number ranged to 10^{11}. Using ink as a tracer, they observed thin laminar boundary layers on the end-walls and relatively inactive cores in the two zones. A thicker boundary layer flowed along the enclosure bottom, and a nearly stagnant region was trapped in the hot zone above the sill of the partition. The formation of a trapped hot pool at the ceiling of the hot room is a consequence of the CWT boundary condition used in these experiments and cannot occur with a CWHF boundary condition.

Nansteel and Greif (30) extended this work to more complex partitions including a doorway, and measured average Nusselt numbers showed good agreement with the experimental results of Weber (26) who used the same configuration but with freon gas. Both studies showed that the heat transfer per unit of doorway area depended only weakly on the doorway width in the partition, a result suggesting that three-dimensional effects may not be important for convection through apertures--a situation that sometimes prevails in buildings as well.

The Nusselt numbers measured by Lin and Bejan (29) for similar configurations are typically 50% less than those reported by Nansteel and Greif (27), and we know of no satisfactory explanation for this discrepancy. Yamaguchi (31) has continued the work of Weber with freon gas in divided enclosures for nine different configurations. He has noted some discrepancies between his work and that of Weber (26) and Weber and Kearney (25). It is clear that these discrepancies must be resolved, and work is continuing at LANL with a new stainless steel enclosure to address this issue. This has no direct bearing on the model proposed in this paper, but it does raise the question as to how one can validate a computational model when there are unexplained discrepancies in the reported experimental measurements.

GENERALIZATIONS BASED ON OBSERVATIONS AND DATA

Figure 1 depicts air flow patterns typical of most of the LANL full-scale passive building measurements. The airflows were visualized using smoke, titanium tetrachloride or helium filled soap bubbles (32). Figure 1 shows a two-room configuration connected by an upper and lower aperture, and while it is simpler than most buildings, it possesses all of the basic phenomena that have been observed. The south room is a double-glazed, solar-heated sunspace with a mass wall on its north side and a massive floor. The north room is the living space with a north wall that loses heat to the outside and may incorporate thermal storage. The flow lines depict the situation near noon on a clear winter day.

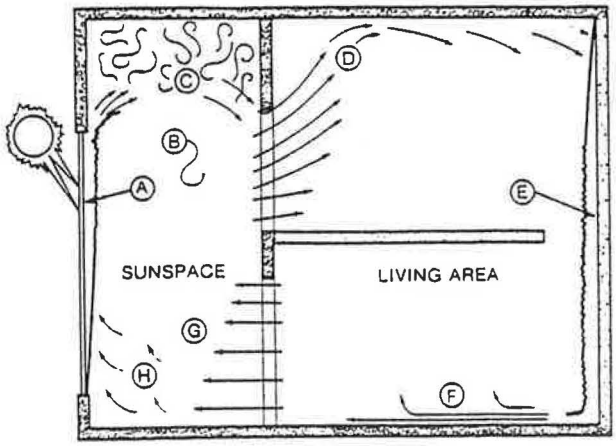

FIG. 1 Sketch of observed airflow in a strongly solar heated passive building (elevation cross-sectional view). Letters designate the following effects:

(A) strong upward boundary-layer flow on the glazing;
(B) weak boundary-layer flows from other warm vertical walls in sunspace;
(C) mixed pool of air above glazing and upper aperture;
(D) warm air passing through the aperture and rising to its own density (or temperature) level;
(E) downward boundary-layer flow on the cool north wall;
(F) cool air stream returning to sunspace;
(G) airflow distribution through lower aperture into the sunspace;
(H) airflow rising as it passes over warm sunspace floor.

With direct sun, the glazing typically operates about 5°C (10°F) warmer than the sunspace air due to solar absorption in the glass. This produces a strong upward boundary-layer flow on the glazing which entrains cool air from the sunspace core. Velocities of 0.46 to 0.61 m/s (1.5 to 2.0 ft/sec) have been measured in the glazing boundary layer. Preliminary estimates lead us to believe that the sunspace glazing accounts for more than half of the heat flow from the sunspace into the remainder of the building during periods of strong solar heating, with the remainder coming from the warm sunspace north wall and floor. The inertia from this vigorous convective flow carries most of the involved air into the space above the top of the glazing and above the upper edge of the upper aperture. There the air mixes somewhat as it travels north and downward toward the upper aperture. The air in this mixed layer is almost isothermal with a tendency for the temperature to be slightly cooler at the top of the layer from heat transfer to the roof (an unstable stratification which would tend to mix). The remaining air in the sunspace core is nearly motionless (away from the apertures) and is always stratified (0.91 to 2.19°C/m or 0.5 to 1.2°F/ft) during periods of significant interzone convection through the apertures. The evidence strongly suggests that convective exchange and stratification are intimately linked, although the dynamics of the processes that occur are not yet completely clear.

Figure 1 suggests the flow in each aperture is one directional. But an aperture often passes flow in both directions simultaneously. The velocity varies as the square root of the vertical distance from a **neutral plane** (defined as the height at which the pressure in both rooms are the same). This relationship was developed by Brown and Solvason (24) for unstratified enclosures, but it has proved to be quite accurate even in stratified situations. For two rooms connected by a single aperture, the location of the neutral plane is approximately at the aperture midheight in order to balance the mass flows.

As warm air passes through the upper aperture to the cooler north room (Fig. 1), it would rise to its own density (or temperature) level. If no match is found, it travels to the ceiling and flows horizontally towards the north wall. The boundary layer on the north wall entrains air from this ceiling flow and from the core, and ejects cold air at the floor level. The cool room is stratified in a manner similar to that of the sunspace with the temperature gradient of the two rooms being nearly equal over the vertical height of the aperture.

The cool stream of air entering the sunspace is warmed by the floor, and in some cases it rises into the sunspace core before reaching the glazing. Normally, no floor thermal plumes are observed during the midday hours of intense heating. But we suspect that plume formation may be significant in late afternoon after the sunspace floor temperature has increased by solar heating.

A more detailed description of the effects observed in the passive buildings that we have monitored is presented by Balcomb (33).

ANALYSIS

Discussion

Based on our flow visualization studies and data obtained for full-scale buildings, we propose a model for heat and airflow in passive solar buildings shown schematically in Fig. 2. The model consists of three basic components: (1) boundary layer equations for heat transfer and air motion at vertical heated or cooled surfaces in the building; (2) orifice equations to model airflow through apertures; and (3) conservation equations for core models (two in this case) to determine core vertical flows and the stratified temperature distribution in the rooms. The boundary layers occur on the solar heated glazing and heated or cooled vertical walls. The core model assumes horizontal isotherms in each zone which is in close agreement with our data for all building types, as well as with the results of others for high Rayleigh numbers (19,34). Heat transfer or subsequent air motion arising from heated or cooled horizontal surfaces are not included in the present version of the model, but Anderson (35) has suggested this to be an important effect. For simplicity, we treat here only one aperture coupling two rooms with heat transfer at the north and south walls, and all other surfaces insulated. The method can be extended to multiple rooms having any number of vertical heat transfer surfaces and apertures.

Referring to Fig. 2, the interaction between the various components is as follows. The cores exchange air through the apertures, and the boundary layers exchange air with the cores (entraining when the boundary layer thickness; ejecting when the

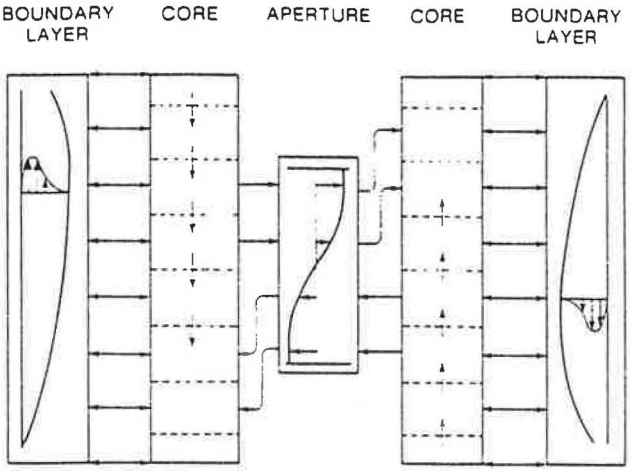

FIG. 2 Schematic diagram of proposed building-convection model depicting interaction among the components.

boundary layer thins). The equations for the three elements of the model--boundary layers, cores and apertures--are interdependent and so must be solved simultaneously.

The proposed model differs from existing nodal-network models in two ways. Firstly, nodal-network models utilize heat transfer coefficients between the walls and the room air; whereas, the proposed model does not. The coefficients which depend on such variables as geometry, thermal boundary conditions, and degree of stratification are usually not available. The proposed model takes account of these variables in determining the heat transport. Secondly, large nodal-network models do not include multiple vertical zones (i.e., no account for stratification); the proposed model includes this as a major feature because of the strong effect of stratification on the heat transfer and thermal comfort. The proposed model provides more detailed information than these methods, namely, the stratification temperature profiles in each room. On the other hand, the proposed model provides less information than existing finite difference codes, because the enclosure has been replaced by boundary layer, core, and aperture models which involve a number of approximations. However, the additional detail given by the finite difference methods is not required for determining thermal performance, and the savings in computing time should be significant.

The boundary layers and the aperture flows are treated as quasi-steady; only the core equations retain the time derivatives. Estimates of time constants for the establishment of flows in these three elements show this to be an accurate assumption for conditions typical of buildings.

Equation Development

Laminar Boundary Layer Equations. Consider the boundary-layer flow of air along a vertical wall in a stratified environment having a variable wall heat flux arising from a combination of a constant heat flux and convection with the ambient (Fig. 3). The integral form of the momentum and energy equations are

$$\frac{d}{dx}\int_0^\delta u^2 dy = g\beta\int_0^\delta (T-T_\infty)dy - \frac{\tau_w}{\rho} \qquad (1a)$$

$$\frac{d}{dx}\int_0^\delta u(T-T_\infty)dy = \frac{q_w}{\rho c_p} - \frac{dT_\infty}{dx}\int_0^\delta u dy \qquad (1b)$$

where the last term in Eq. (1b) allows for a stratified core. For laminar flow

$$q_w = -k\left(\frac{\partial T}{\partial y}\right)_{y=0} \; ; \; \frac{\tau_w}{\rho} = \nu\left(\frac{\partial u}{\partial y}\right)_{y=0} \qquad (2)$$

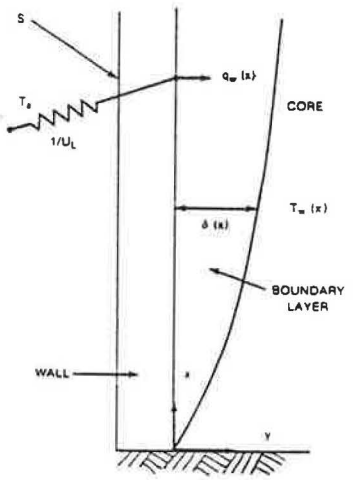

FIG. 3 Boundary-layer flow over a vertical wall in a stratified medium with heat loss to the ambient (at T_a) and a constant incident flux (S).

We take the usual boundary conditions (36) to apply here, which ignore the small core velocity, and the appropriate velocity and temperature fields in the boundary layer are

$$\frac{u}{\omega} = \eta(1-\eta)^2 \qquad (3a)$$

and

$$T - T_\infty = \left[\frac{\alpha_e S - U_L(T_\infty - T_a)}{U_L + \frac{2k}{\delta}}\right][1-\eta]^2 \qquad (3b)$$

respectively.

With Eqs. (2) and (3), Eqs. (1) are written as

$$I_{\ell 1}\frac{d}{dx}(\omega^2\delta) = I_{\ell 2} g\beta f(x)\frac{\delta^2}{\left(1+Nu_L\frac{\delta}{H}\right)} - \nu\frac{\omega}{\delta} \qquad (4a)$$

$$I_{\ell 3}\, f(x)\left[\frac{d}{dx}(\omega\delta^2) - \frac{\omega\delta^2 Nu_L}{H - Nu_L\delta}\frac{d\delta}{dx}\right]$$

$$= 2\kappa f(x) + (I_{\ell 3} - I_{\ell 4})\frac{Nu_L}{H}\omega\delta^2\frac{dT_\infty}{dx} - I_{\ell 4}\omega\delta\frac{dT_\infty}{dx} \qquad (4b)$$

respectively, where

$$f(x) \equiv \frac{\alpha_e S}{2k} - Nu_L\frac{T_\infty - T_a}{H} \qquad (5)$$

and

$$Nu_L \equiv \frac{U_L H}{2k} \qquad (6)$$

The coefficients, $I_{\ell i}$, have the values 1/105, 1/3, 1/30 and 1/12 for i=1,2,3,4 respectively.

Equations (4) are appropriately scaled by considering a balance between the convection and conduction terms in the energy equation, and a balance between the viscous and buoyancy terms in the momentum equation. From these we obtain

$$\lambda \equiv \frac{\delta Ra^{1/5}}{H} \; ; \quad \xi \equiv \frac{x}{H} \; ; \quad \Omega \equiv \frac{\omega H}{\kappa Ra^{2/5}} \; ;$$
$$\theta \equiv \frac{k(T_\infty - T_a)}{\alpha_e SH} \; ; \quad Ra \equiv \frac{g\beta H^4 \alpha_e S}{\nu\kappa k} \qquad (7)$$

Before scaling Eqs. (4), the derivatives on their left sides are expanded and the equations are combined to give two differential equations--one in λ^5 and the other in $\Omega^{5/3}$. These quantities vary linearly with ξ near the origin (for CWHF) making the numerical solution well behaved there.

The final dimensionless laminar boundary layer equations become

$$\frac{3}{5}\left[\frac{3+N\lambda}{1+N\lambda}\right]\frac{d\Omega^{5/3}}{d\xi} = \frac{PrI_{\ell 2}(0.5-Nu_L\theta)(2+N\lambda)}{I_{\ell 1}(1+N\lambda)^2 B_\ell^{2/5}} - \left[\frac{Pr(2+N\lambda)}{I_{\ell 1}(1+N\lambda)} + \frac{2}{I_{\ell 3}}\right]B_\ell^{4/5}$$
$$-\left[\left(1-\frac{I_{\ell 4}}{I_{\ell 3}}\right)Nu_L\lambda - \frac{I_{\ell 4}}{I_{\ell 3}}Ra^{1/5}\right]\frac{B_\ell^2\lambda^4\frac{d\theta}{d\xi}}{0.5 - Nu_L\theta} \qquad (8a)$$

$$\frac{1}{5}\left[\frac{3+N\lambda}{1+N\lambda}\right]\frac{d\lambda^5}{dx} = \left[\frac{Pr}{I_{\ell 1}} + \frac{4}{I_{\ell 3}}\right]B_\ell^{-6/5} - \frac{Pr\, I_{\ell 2}(0.5-Nu_L\theta)}{I_{\ell 1}(1+N\lambda)B_\ell^{12/5}}$$
$$+\left[\left(1-\frac{I_{\ell 4}}{I_{\ell 3}}\right)Nu_L\lambda - \frac{I_{\ell 4}}{I_{\ell 3}}Ra^{1/5}\right]\frac{\lambda^4\frac{d\theta}{d\xi}}{1-2Nu_L\theta} \qquad (8b)$$

where

$$B_\ell^2 \equiv \frac{\Omega^{5/3}}{\lambda^5} \qquad (9)$$

and

$$N \equiv \frac{Nu_L}{Ra^{1/5}} \qquad (10)$$

In the limit as $\xi \to 0$, an estimate of $B_\ell(0)$ is obtained by using the approximation $\lambda(0) = 0$ yielding

$$B_\ell(0) = \left[\frac{PrI_{\ell 2}\left[0.5-Nu_L\theta(0)\right]}{Pr + 14\frac{I_{\ell 1}}{5 I_{\ell 3}}}\right]^{5/6} \qquad (11)$$

Turbulent Boundary Layer Equations. A similar procedure is followed for turbulent flow. Equations (1) remain unchanged. But the wall shear stress and heat flux are now evaluated using the Blasius Equation (37) and Reynold's analogy (38) following the usual procedure (18,22). Thus

$$\frac{\tau_w}{\rho} = I_{t5}\omega^2\left(\frac{\nu}{\omega\delta}\right)^{2/(n+1)}$$

$$\frac{q_w}{\rho c_p} = \frac{\left(\frac{\tau_w}{\rho}\right)}{\omega Pr^{2/3}} \tag{12}$$

where n is an adjustable constant. For the usual case of n = 7 the exponent for the last term becomes 1/4. We will take $I_{t5} = 0.0225$. The velocity and temperature profiles are taken to be

$$\frac{u}{\omega} = \eta^{1/n}(1-\eta)^4 \tag{13a}$$

$$T - T_\infty = \frac{\left[\alpha_e S - U_L(T_\infty - T_a)\right](1-\eta^{1/n})}{U_L + I_{t5}Pr^{-2/3}(\rho c_p \omega)\left(\frac{\nu}{\omega\delta}\right)^{2/(n+1)}} \tag{13b}$$

Following the same procedure that was used for the laminar equations, we seek dimensionless boundary layer equations for λ^q and Ω^r where q and r are selected so that these quantities are linear near the origin. We obtain

$$\frac{C_8}{B_t r}\frac{d\Omega^r}{d\xi} = C_1 C_6 B_t^{(a-3)/r} - \frac{(C_2C_6 - C_3)}{B_t^{a/r}} \tag{14a}$$

$$- C_4\lambda^q + C_5 B_t^{(1-a)/r}\,\lambda^{4/(3-2a)}$$

$$\frac{C_8}{q}\frac{d\lambda^q}{d\xi} = -C_1 C_7 B_t^{(a-3)/r} + \frac{C_2C_7 + 2C_3}{B_t^{a/r}} + 2\,C_4\lambda^q \tag{14b}$$

$$-2\,C_5 B_t^{(1-a)/r}\,\lambda^{4/(3-2a)}$$

where

$$B_t \equiv \frac{\Omega^r}{\lambda^q} \tag{15}$$

and

$$a \equiv \frac{2}{n+1}\ ;\ q \equiv \frac{3n+7}{3n-1}\ ;\ r \equiv \frac{3n+7}{n+5} \tag{16}$$

In Eqs. (14) the coefficients are

$$C_1 \equiv \frac{\frac{(1-2Nu_L\theta)Pr\ I_{t2}\ Ra^{1/5}}{I_{t1}}}{I_{t5}Pr^{(a-2/3)}Ra^{(2-a)/5} + \frac{2Nu_L}{\Omega^{1-a}\lambda^a}} \tag{17a}$$

$$C_2 \equiv \frac{I_{t5}\ Pr^a}{I_{t1}Ra^{(a-1)/5}} \tag{17b}$$

$$C_3 \equiv \frac{I_{t5}\ Pr^{a-2/3}}{Ra^{(a-1)/5}I_{t3}} \tag{17c}$$

$$C_4 \equiv \frac{2\left(1 - \frac{I_{t4}}{I_{t3}}\right)Nu_L\left(\frac{d\theta}{d\xi}\right)}{1 - 2\,Nu_L\theta} \tag{17d}$$

$$C_5 \equiv \frac{I_{t4}I_{t5}Ra^{(2-a)/5}Pr^{(a-2/3)}\frac{d\theta}{d\xi}}{I_{t3}(1-2\,Nu_L\theta)} \tag{17e}$$

$$C_6 \equiv \frac{(1+a)I_{t5}Ra^{(2-a)/5}Pr^{(a-2/3)} + 2\,Nu_L\Omega^{a-1}\lambda^a}{I_{t5}Ra^{(2-a)/5}Pr^{(a-2/3)} + 2\,Nu_L\Omega^{a-1}\lambda^a} \tag{17f}$$

$$C_7 = \frac{a\,I_{t5}Pr^{(a-2/3)}Ra^{(2-a)/5} + 2\,Nu_L\Omega^{a-1}\lambda^a}{I_{t5}Pr^{(a-2/3)}Ra^{(2-a)/5} + 2\,Nu_L\Omega^{a-1}\lambda^a} \tag{17g}$$

$$C_8 = 2\,C_6 - C_7 \tag{17h}$$

The values for I_t, a, q, and r are given in Table 1 for a range of n values.

TABLE 1

n	$I_{t1}x10^2$	I_{t2}	$I_{t3}x10^2$	I_{t4}	a	q	r
3	2.1850	.2500	4.4446	.1001	.5000	2.0000	2.0000
4	3.1530	.2000	4.3794	.1177	.4000	1.7272	2.1111
5	3.9723	.1667	4.1659	.1301	.3333	1.3571	2.2000
6	4.6571	.1429	3.9137	.1393	.2828	1.4706	2.2727
7	5.2315	.1250	3.6631	.1464	.2500	1.4000	2.3333
8	5.7172	.1111	3.4285	.1520	.2222	1.3478	2.3846

In the limit $\xi \to 0$, an estimate of $B_t(0)$ is obtained as before

$$B_t(0) = \left[\frac{\frac{q(C_2+2C_3)}{r} + C_2 + C_3}{C_1\left(1 + \frac{q}{r}\right)}\right]^{r/(2a-3)} \tag{18}$$

An interesting result is found from Eq. (14) by setting their left sides to zero. The equations show that for a nonzero constant stratification temperature gradient, the boundary layer assumes a constant thickness given by

$$\lambda = \left\{(C_4/C_3)B_t^{1/r} - (C_5/C_3)B_t^{a/r}\lambda^{(q+4/(2a-3))}\right\}^{(2a-3)/4} \tag{19}$$

where

$$B_t = \left(\frac{C_2}{C_1}\right)^{r/(2a-3)}$$

The same result was obtained by Gill (16) for a CWHF vertical wall and by Kimura and Bejan (17) for convection in a vertical enclosure in both cases using the Oseen linearization, a procedure entirely different from our integral approach.

Core Equations

Each core is divided into horizontal cells of plan area $L_j D_j$ and thickness Δx with the temperature, pressure, vertical and horizontal flows all defined at the bottom of each cell. The cell labeling convention and identification of properties are shown in Fig. 4.

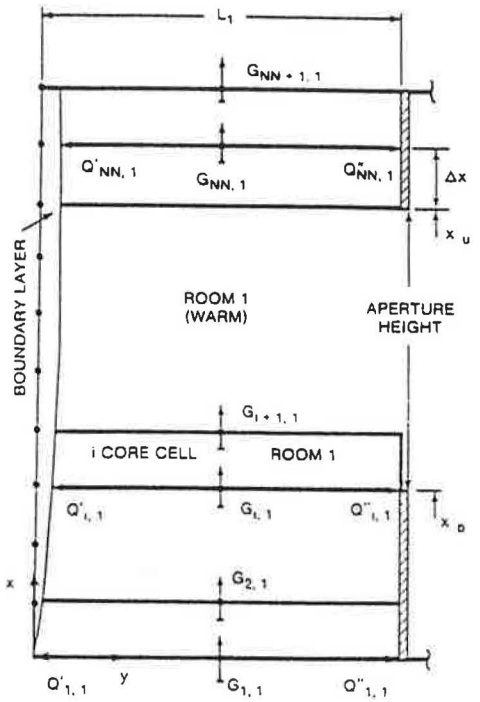

FIG. 4 Cell geometry and property identification for core model (elevation view).

The mass and energy conservation equations for the i'th cell in the j'th room are written as

$$D_j L_j \Delta x \frac{d}{dt}(\rho_{i,j}) = \rho_{i-1,j} G_{i,j} - \rho_{i,j} G_{i+1,j} - \rho_{i,j} Q'_{i,j} - \rho_{i,j} Q''_{i,j} \tag{20a}$$

$$D_j L_j \Delta x \frac{d}{dt}(\rho_{i,j} c_p T_{i,j}) = D_j L_j \Delta x k \frac{T_{i+1,j}+T_{i-1,j}-2T_{i,j}}{\Delta x^2} + c_p\{G_{i,j}T_{i-1,j}\rho_{i-1,j} - G_{i+1,j}T_{i,j}\rho_{i,j} - (Q'_{i,j}+Q''_{i,j})\rho_{i,j}T_{i,j}\} \tag{20b}$$

From hydrostatics the pressure distribution is given by

$$p = p_o + \rho g x \tag{21}$$

and with the ideal gas equation of state we can write

$$\frac{\rho T}{\rho_o T_o} = \frac{p}{p_o} = 1 + \frac{\rho_o g x}{p_o} \tag{22}$$

Taking as typical values $\rho_o g = 11.8$ n/m^3 (0.075 lb/ft^3), $x = 3$ m (9.8 ft), and $p_o = 10^5$ Pa (14.5 psia), it is evident that the last term is negligible (3 parts in 10,000), and we can set

$$\rho T = \rho_o T_o \tag{23a}$$

and

$$d\rho = -\left(\frac{\rho_o T_o}{T^2}\right) dT \tag{23b}$$

With Eqs. (23), mass and energy conservation for a core cell are written in dimensionless form as follows[1]

$$\frac{d\psi_{i,j}}{d\tau} = \frac{(A_L A_D)_j}{\Delta\xi}\{\psi^2_{i,j}\left[\frac{\hat{G}_{i+1,j}}{\psi_{i+k1,j}} - \frac{\hat{G}_{i,j}}{\psi_{i-1+k0,j}}\right] + \psi_{i,j}(\hat{Q}'_{i,j}+\hat{Q}''_{i,j})\} \tag{24a}$$

$$0 = \hat{G}_{i,j} - (\hat{Q}''_{i,j}+\hat{Q}'_{i,j}) - \hat{G}_{i+1,j} + \frac{\{\psi_{i+1,j}+\psi_{i-1,j}-2\psi_{i,j}\}}{A_{Lj}\Delta\xi} \tag{24b}$$

A surprising consequence of Eq. (23a) is that the energy equation (24b) determines the flow distribution, and the continuity equation (24a) determines the temperature distribution.

The core boundary conditions are: (1) ceiling, floor and partitions are impermeable to mass and heat flow; (2) boundary layer flows are entrained from the core horizontally; and (3) aperture outflows are drawn horizontally while inflows rise or fall to their appropriate temperature level.

Aperture Model Aperture flows are driven by pressure differences that arise from different vertical temperature distributions in each room. Equation (22) states that to first-order the pressure is constant everywhere. Here, however, we are considering aperture flows that originate because of second-order inbalances in pressure between the two rooms. Equation (21) is written in dimensionless form for both the warm and cool room, and the difference between them becomes

$$\hat{p}_1(\xi) - \hat{p}_2(\xi) = \hat{p}_{01} - \hat{p}_{02} - 2\int_0^{\xi}\left[\frac{1}{\psi_1(\zeta)} - \frac{1}{\psi_2(\zeta)}\right]d\zeta \tag{25}$$

where p_{01} and p_{02} are the reference pressure in each room taken at the floor level.

The local volumetric flowrate, Q", over cell thickness Δx and aperture breadth, W, may now be given by the Brown and Solvason (24) invicid orifice equation expressed here in dimensionless form

[1]Here the indices k1 and k0 are included to properly account for upward and downward convection. k1 = k0 = 1 for downflow and 0 for upflow).

$$\hat{Q}''(\xi) = C_d A_{wj} \Delta\xi \sqrt{\frac{RaPr}{\beta T_o}} \left\{ \psi_s(\xi) \left[P_{01} - P_{02} - 2 \int_0^{\xi} \left(\frac{1}{\psi_1(\zeta)} - \frac{1}{\psi_2(\zeta)} \right) d\zeta \right] \right\}^{1/2} \quad (26)$$

where the subscript s denotes the source room (s=1 for flow from warm to cool; s=2 for the reverse). The orifice coefficent, C_d, is taken to be 0.611.

Reference pressure P_{01} may be considered arbitrary, whereas P_{02} is determined relative to P_{01} such that integral continuity is satisfied across the aperture. Thus

$$\int_{\xi_b}^{\xi_u} \frac{1}{\psi_j(\xi)} \hat{Q}''(\xi) d\xi = 0 \quad (27)$$

Equation (27) is solved iteratively by equating it to a residual, R. We then write

$$\hat{P}_{02}\Big|_{new} = \hat{P}_{02}\Big|_{old} + RC_r$$

$$\hat{P}_{01}\Big|_{new} = \hat{P}_{01}\Big|_{old} - RC_r \quad (28)$$

A value of 2×10^{-7} for the relaxation factor, C_r, provides convergence in about 5 iterations.

Definition of Nusselt Number

A local Nusselt number is defined as

$$Nu_x \equiv \frac{q_w H}{k \overline{\Delta T}} \quad (29)$$

where $\overline{\Delta T}$ is the overall temperature difference between the walls in the warm and cool room measured at the same height. For laminar flow this becomes

$$Nu_x = \frac{E_1(\xi)}{E_2(\xi) + E_2(1-\xi) + \psi_1(\xi) - \psi_2(1-\xi)} \quad (30a)$$

where

$$E_1(\xi) = \frac{1 - 2\,Nu_L \theta(\xi)}{1 + Nu_L \lambda(\xi)}$$

$$E_2(\xi) = \frac{(0.5 - Nu_L \theta(\xi))\lambda(\xi)}{(1 + N\lambda(\xi)) Ra^{1/5}}$$

For turbulent flow, the local Nusselt number is

$$Nu_x = \frac{\frac{E_3(\xi)E_5(\xi)}{E_3(\xi) + E_4}}{\frac{E_5(\xi)}{E_3(\xi) + E_4} + \frac{E_5(1-\xi)}{E_3(1-\xi) + E_4} + \psi_1(\xi) - \psi_2(1-\xi)} \quad (30b)$$

where

$$E_3(\xi) = \frac{I_{t5} Pr^{(a-2/3)}}{Ra^{(a-1)/5} \Omega^{a-1} \lambda a}$$

$$E_4 = 2\,Nu_L$$

$$E_5(\xi) = 1 - 2\,Nu_L \theta(\xi)$$

Method of Solution

Once initial temperatures for the two rooms are prescribed, the boundary layer equations are solved using a fourth-order Runge Kutta method with $\Delta\xi = 0.05$ (21 nodes). The solution of the boundary layer equations provides the Q' distribution. Next, the pressure distribution is determined for each core by solving of Eq. (25), and the aperture flows, Q", are then calculated using Eq. (26). The direction of aperture flows determines their origin (whether from the warm or cool room), and their destination is determined by scanning the cells in the opposite room to find the two adjacent cells that bound the temperature of the Q" flow. The flow is then divided linearly between these two cells so as to maintain energy conservation.

Having determined the Q' and Q" distributions for each core, the vertical flows (the G's) are then calculated using Eq. (24b), and the core temperatures are updated using Eq. (24a).

The residual R is calculated from Eq. (27). If it is small enough time is incremented. If not, the pressures are adjusted using Eq. (28), and the above procedure is repeated at the same time step until suitable convergence of R is achieved. Presently, $R < 0.01 Q''_{min}$ is assumed to satisfy integral continuity.

RESULTS AND DISCUSSION

We consider a building with an adiabatic partition separating two air-filled rooms, each with height/length=2 and height/breadth=1. An aperture in the partition has a height of 0.5H, a breadth of 0.25H, with its lower sill located at x=0.25H. The rooms are initially linearly stratified with a temperature difference of 0.0056°C (0.01°F) from ceiling to floor, and the cool room is 0.56°C (1°F) cooler than the warm room at any level. At t=0 when the aperture is opened, flow is immediately established because of Eq. (27), and the computation predicts the evolution of the flow and the stratification temperature profiles with time. Two cases are considered. Case 1: All surfaces are adiabatic. Case 2: All surfaces are adiabatic except that the south wall is heated, and the north wall is cooled, both with constant heat flux. For simplicity we assume that the boundary layers are turbulent with n=7. For both cases, $\Delta\tau = 10^{-5}$ and $\Delta\xi = 0.05$. For Case 2, $Ra = 10^{12}$ which corresponds to H=2.4 m (8 ft) and a solar input of 31.5 w/m^2 (10 Btu/hr ft^2).

The results for Case 1 are shown in Figs. 5-7. The temperature at the bottom of the warm room decreases in the expected manner (Fig. 5), as air from the cool room flows in through the bottom of the aperture (and conversely for the cool room). Vertical heat conduction in the cores has a negligible role in this process, with a time constant of 70 hours for H=2.4 m (8 ft). We know from observations that there is some turbulent core mixing, but we

have made no attempt to include it at this time for lack of information. The net effect of the flow is to increase the stratification in each room, and ultimately the same nonlinear temperature profile is approached in each room. For H=2.4 m (8 ft), the three dimensionless times would correspond to 0.72, 2.15 and 4.47 minutes. The aperture flow distributions (Fig. 6) decay with time approximately exponentially with a time constant of about 5×10^{-4} based on the total one-way flow (corresponding to 2 minutes for H=2.4 m).

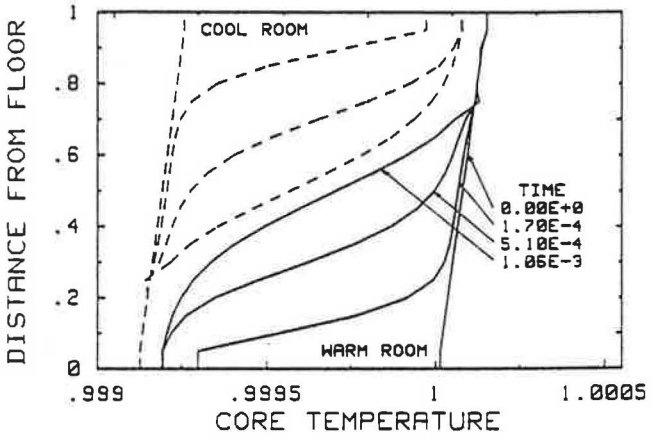

FIG. 5 Vertical temperature distributions (ψ vs ξ) in the warm and cool rooms at three times after the opening of the aperture for Case 1 (adiabatic end-walls).

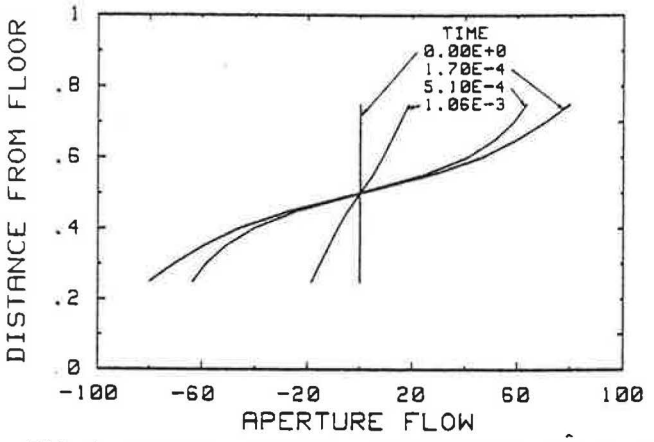

FIG. 6 Aperture flowrate distributions ($\hat{Q}$" vs ξ) for Case 1.

The vertical core flow in the warm room (Fig. 7) is always zero for $x > 0.75$, since flow from the warm room is trapped above the aperture upper sill. The vertical flow distributions are quite different for the three times. At $\tau = 1.7 \times 10^{-4}$, the cold inflow drops directly to the floor of the warm room, since it is colder than the air at floor level. Cells 2 to 10 have no horizontal flows (no Q' nor Q"), and so the core flow (G) remains constant in that range (a "slug flow"). From $0.5 < x < 0.75$, the vertical core flow drops to zero as the warm-room core delivers horizontal flow to the cold

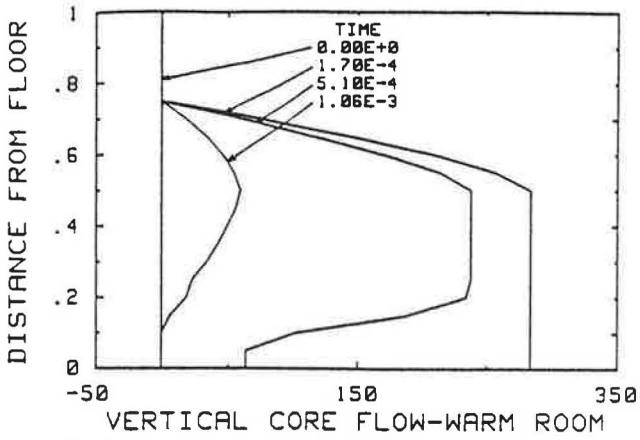

FIG. 7 Warm-room vertical flowrate distributions ($\hat{G}$ vs ξ) for Case 1.

room via the aperture. For $\tau = 5.1 \times 10^{-4}$, only a portion of the cold inflow drops to the floor; the remainder enters the core at corresponding temperature levels. There still remains a region ($0.2 < x < 0.5$) of "slug flow" since fluid from the cold room has no temperature correspondence in this range. At $\tau = 10.6 \times 10^{-4}$, there is no region of slug flow, and both the upper and lower regions of both rooms have become stagnant.

Now turning to Case 2 with end-wall heating and cooling, the warm room temperature distribution (Fig. 8) is quite different from Case 1 (Fig. 5). The warm room is hotter at the ceiling due to the rising warm boundary-layer flow. And it is colder at the floor, since the inflow from the cold room is colder due to the influence of the cooled-wall boundary layer. The net result is a substantial increase in stratification. The aperture flow (Fig. 9) drops only slightly, showing that the wall heat flux was almost sufficient to maintain the room temperature difference. The boundary-layer thickness (Fig. 10) goes through a rather major adjustment responding to the change in the stratification. Note that the boundary layer actually decreases in thickness over a substantial fraction of its length. It is worth noting that many writers describe the boundary layer as entraining along its entire length, and ejecting only at its downstream end; but in stratified flows the boundary layer can shrink, and this is especially prominent with a CWT boundary condition. This has important implications to the "feeding" of the core (which will not be pursued here) and to the establishment of the stratification temperature profile. At $\tau > 5.1 \times 10^{-4}$, instabilities are encountered in the boundary-layer calculation that seem to be associated with the steepness of the core temperature distribution. As suggested by a referee, it is probably related to our use of an explicit integration scheme, and the stability criterion for this system of equations should be investigated.

CONCLUSIONS AND RECOMMENDATIONS

A transient two dimensional model for interzone heat transfer in passive solar buildings has been developed and used to predict transient room core temperatures, heat transfer, and airflow through apertures for two cases. Results from the model are in general agreement with the data. We have

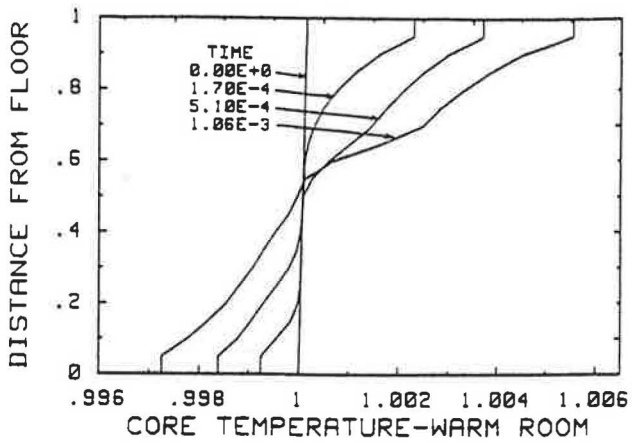

FIG. 8 Vertical temperature distributions (ψ vs ξ) in the warm room at three times after the opening of the aperture for Case 2 (end-wall heating and cooling).

measured maximum aperture velocities of about 0.09 m/s (17 ft/min) for room-to-room temperature differences of 0.56°C (1°F) (33), and from Fig. 9 we compute maximum velocities that range from 0.07 to 0.08 m/s (12.5 to 14.4 ft/sec) for comparable conditions. From Fig. 8 core temperature gradients range from 1.53 to 2.51°C/m (0.84 to 1.38°F/ft), which are in good agreement with typical values obtained for full-scale passive buildings.

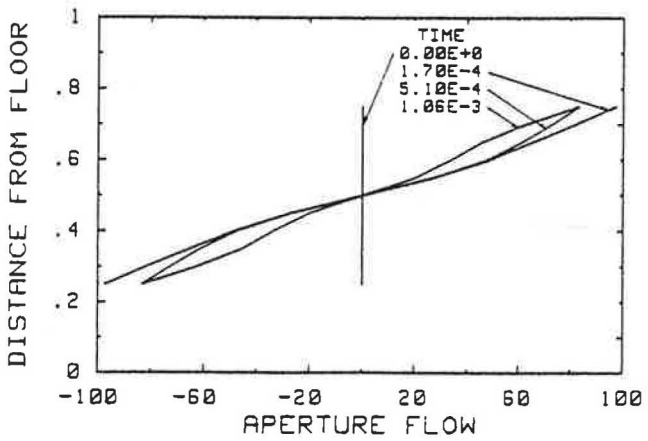

FIG. 9 Aperture flowrate distribution ($\hat{Q}$" vs ξ) for Case 2.

Generality of the model can be improved by including the effects of heat transfer at horizontal surfaces such as floors and ceilings. The convective heat transfer from these surfaces may account for a significant fraction of the energy flow from the sunspace during those hours where the glazing is not directly solar heated.

The implicit integration with respect to time should be replaced by a more stable procedure that will allow the use of larger time steps in the calculation.

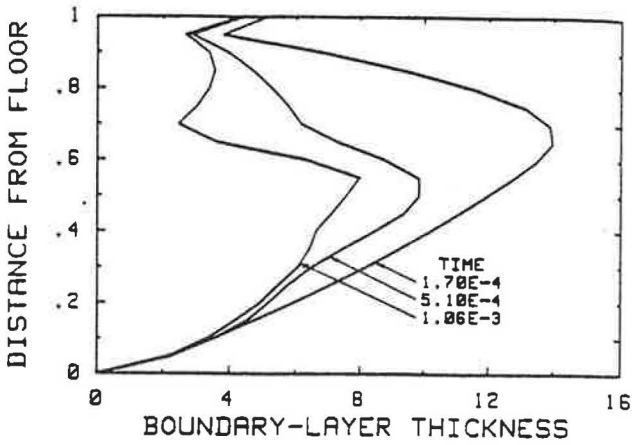

FIG. 10 Warm-room boundary-layer thickness (λ vs ξ) for Case 2.

ACKNOWLEDGEMENTS

This work was performed under the auspices of the United States Department of Energy, Office of Solar Heat Technologies. The authors acknowledge Kenjiro Yamaguchi and Mark White for their assistance in monitoring buildings. The authors appreciate the helpful remarks of a referee relating to the question of stability. The manuscript was typed by Mary Stampfli at University of Wisconsin-Madison.

REFERENCES

1. Balcomb, J.D. and K. Yamaguchi, "Heat Distribution by Natural Convection", Proc. 8th Passive Solar Conf., Santa Fe, NM, Sept. 7-9, 1983 (LA-UR-83-1872).
2. Balcomb, J.D., G.F. Jones and K. Yamaguchi, "Natural Air Motion and Stratification in Passive Buildings", Passive and Hybrid Solar Energy Update, Washington, D.C., Sept. 5-7, 1984 (LA-UR-84-2650).
3. Balcomb, J.D. and G.F. Jones, "Natural Air Motion in Passive Solar Buildings", Solar Buildings: Realities for Today, Trends for Tomorrow, Washington, D.C., March 18-20, 1985 (LA-UR-85-1045).
4. Balcomb, J.D., G.F. Jones and K. Yamaguchi, "Natural Convection Airflow Measurement and Theory", 9th Nat. Passive Solar Conf., Columbus, OH, Sept. 24-26, 1984 (LA-UR-84-2639).
5. Hill, D., A. Kirkpatrick and P. Burns, "Interzonal Natural Convection Heat Transfer in a Passive Solar Building", To be presented at the 23rd AIChE/ASME National Heat Transfer Conference, Denver, Colorado, August, 1985.
6. Batchelor, G.K., "Heat Transfer by Free Convection Across a Closed Cavity Between Vertical Boundaries at Different Temperatures", Quart. Appl. Math. 12, 1954, pp. 209-233.
7. Elder, J.W., "Laminar Free Convection in a Vertical Slot", J. Fluid Mech. 23, 1965, pp. 7-11.
8. Eckert, E.R.G. and W.O. Carlson, "Natural Convection in an Air Layer Enclosed Between Two Vertical Plates with Different Temperatures", Int. J. Ht. and Mass T. 2, 1961, pp. 106-120.

9. Wilkes, J.O. and S.W. Churchill, "The Finite-Difference Computation of Natural Convection in a Rectangular Enclosure", AIChE J. 12, 1966, pp. 161-166.
10. Rubel, A. and F. Landis, "Numerical Study of Natural Convection in a Vertical Rectangular Enclosure", Phys. Fluids Supplement II 12, 1969, pp. II-208-213.
11. Gershuni, G.Z., E.M. Zhukhovitskii and E.L. Tarunin, "Numerical Investigation of Convective Motion in a Closed Cavity", Izv. AN SSSR, Mekhanika Zhidkosti i Gaza 1, 1966, pp. 56-62.
12. Quon, C., "High Rayleigh Number Convection in an Enclosure--A Numerical Study", Phys. Fluids 15, 1972, pp. 12-19.
13. Strada, M. and J.C. Heinrich, "Heat Transfer Rates in Natural Convection at High Rayleigh Numbers in Rectangular Enclosures: A Numerical Study", Num. Ht. Trans. 5, 1982, pp. 81-93.
14. De Vahl Davis, G., "Natural Convection of Air in a Square Cavity: A Bench Mark Numerical Solution", Int. J. Numerical Methods Fluids 3, 1983, pp. 249-264.
15. Schinkel, W.M.M., S.J.M. Linthorst and C.J. Hoogendoorn, "The Stratification in Natural Convection in Vertical Enclosures", J. Heat Transfer 105, 1983, pp. 267-272.
16. Gill, A.E., "The Boundary-Layer Regime for Convection in a Rectangular Cavity", J. Fluid Mechanics 26, 1966, pp. 515-536.
17. Kimura, S. and A. Bejan, "The Boundary Layer Natural Convection Regime in a Rectangular Cavity with Uniform Heat Flux from the Side", J. Heat Transfer 106, 1984, pp. 98-103.
18. Evans, L.B., R.C. Reid and E.M. Drake, "Transient Natural Convection in a Vertical Cylinder", AIChE Journal 14, 1968, pp. 251-259.
19. Markatos, N.C. and C.A. Pericleous, "Laminar and Turbulent Natural Convection in an Enclosed Cavity", Proc. ASME National Heat Transfer Conf., Seattle, July 24-28, 1983, pp. 59-68.
20. Bauman, F., A. Gadgil, R., Kammerud and R. Greif, "Buoyancy-Driven Convection in Rectangular Enclosures: Experimental Results and Numerical Calculations", ASME Paper No. 80-HT-66 (ASME, New York, NY, 1980).
21. Gadgil, A., F. Bauman, E. Altmayer and R.C. Kammerud, "Verification of a Numerical Simulation Technique for Natural Convection", J. Heat Transfer 106, 1984, pp. 366-369.
22. Emery, A.F. and N.C. Chu, "Heat Transfer Across Vertical Layers", J. Ht. Trans. 87, 1965, pp. 110-114.
23. MacGregor, R.K. and A.F. Emery, "Free Convection Through Vertical Plane Layers-Moderate and High Prandtl Number Fluids", J. Heat Transfer 91, 1969, pp. 391-403.
24. Brown, W.G. and Solvason, K.R., "Natural Convection Through Rectangular Openings in Partitions, Part I: Vertical Partitions", Int. J. Heat and Mass Transfer 5, 1962, pp. 859-868.
25. Weber, D.D. and R.J. Kearney, "Natural Convective Heat Transfer Through an Aperture in Passive Solar Buildings", Proc. 5th National Passive Solar Conf., Oct. 19-26, 1980, Amherst.
26. Weber, D.D., "Similitude Modeling of Natural Convection Heat Transfer Through an Aperture in Passive Solar Heated Buildings", PhD Thesis, University of Idaho, Moscow, Idaho (LA-8385-T).
27. Nansteel, M.W. and R. Greif, "Natural Convection in Undivided and Partially Divided Rectangular Enclosures", J. Heat Transfer 103, pp. 623-629, 1981.
28. Bajorek, S.M. and J.R. Lloyd, "Experimental Investigation of Natural Convection in Partitioned Enclosures", J. Heat Transfer 104, 1982, pp. 527-532.
29. Lin, N.N. and A. Bejan, "Natural Convection in a Partially Divided Enclosure", Int. J. Ht. and Mass Transfer 26, 1983, pp. 1867- 1878.
30. Nansteel, M.W. and R. Greif, "An Investigation of Natural Convection in Enclosures with Two- and Three-Dimensional Partitions", Int. J. Heat and Mass Transfer 27, 1984, pp. 561-571.
31. Yamaguchi, K., "Experimental Study of Natural Convection Heat Transfer Through an Aperture in Passive Solar Heated Buildings", Proc. 9th Nat. Passive Solar Conf., Columbus, OH, Sept. 24-26, 1984 (LA-UR-84-2638).
32. White, M.D., A.T. Kirkpatrick and C.B. Winn, "Flow Visualization of Interzonal Flow in Passive Solar Structures", Proc. ASME Solar Energy Division Meeting, Knoxville, Tennessee, March 25-28, 1985.
33. Balcomb, J.D., "Heat Distribution by Natural Convection: Interim Report", Los Alamos National Laboratory report in preparation.
34. Sernas, V. and E.I. Lee, "Heat Transfer in Air Enclosures of Aspect Ratio Less Than One", J. of Heat Transfer 103, 1981, pp. 617-622.
35. Anderson, R., E.M. Fisher and M. Bohn, "Natural Convection in a Closed Cavity with Variable Heating of the Floor and One Vertical Wall", Submitted to Int. J. Heat Mass Transfer, 1985.
36. Burmeister, L.C., Convective Heat Transfer, John Wiley and Sons, NY, pp. 525-526, 1983.
37. Burmeister, L.C., Convective Heat Transfer, John Wiley and Sons, NY, pp. 417, 1983.
38. Burmeister, L.C., Convective Heat Transfer, John Wiley and Sons, NY, pp. 541, 1983.